Linear and non-linear electrical dependency of carbon nanotube reinforced composites to internal damage

2015 IOP Conf. Ser.: Mater. Sci. Eng. 74 012002

(http://iopscience.iop.org/1757-899X/74/1/012002)

Linear and non-linear electrical dependency of carbon nanotube reinforced composites to internal damage

D Bekas[1], **SA Grammatikos**[2], **C Kouimtzi**[1], **AS Paipetis**[1]

[1] Dept. of Materials Science & Engineering, University of Ioannina, 45110 Ioannina, Greece.
[2] Dept. of Architecture and Civil Engineering, University of Bath, Bath BA27AY, UK.

paipetis@cc.uoi.gr

Abstract. Carbon nanotube (CNT) enhanced composite materials have attracted the interest of many scientists worldwide, especially in the aerospace industry. Fundamental to their qualification as materials in primary aircraft structures is the investigation of the relationship between their functional characteristics and their long-term behaviour under external combined loads. Conductive reinforcement at the nanoscale is by definition multifunctional as it may *(i)* enhance structural performance and *(ii)* provide structural health monitoring functionalities. It is now well established that reversible changes in the electrical resistance in nano composites are related to strain and irreversible monotonic changes are related to cumulative damage in the nano composite. In this study, the effect of damage in the hysteretic electrical behaviour of nano-enhanced reinforced composites was investigated. The nanocomposites were subjected to different levels of damage and their response to a cyclic electrical potential excitation was monitored as a function of frequency. Along with the dynamic electrical investigation, an Electrical Potential Mapping (EPM) technique was developed to pin-point artificial damage in CNT-enhanced matrix composite materials. The electrical potential field of the bulk material has shown to be characteristic of its internal structural state. The results of EPM technique were contradicted and validated with conventional C-scans.

1. Introduction

Carbon nanotubes (CNTs) possess a unique combination of mechanical, electrical, and thermal properties that makes them excellent candidates to substitute or complement the conventional nano-fillers in the fabrication of multifunctional polymer nano-composites [1-6], mainly in the field of aerospace industry. During the past decade, epoxy resin-based CNT composites were extensively studied by many researchers for their electrical properties [7-11]. It was well established that, these composites could potentially be used for transparent conductive coatings, electrostatic dissipation, electrostatic painting and electromagnetic interference shielding applications..

When employed as an indicator for structural integrity of a component; the electrical properties of composite materials are capable of achieving a direct correlation between the internal damage and the inherent properties. Many researchers managed to relate irreversible electrical resistance change to internal damage of the composite material [12-17]. The structural integrity of Carbon Fiber Reinforced Polymers (CFRPs) with Multi Wall Carbon NanoTubes (MWCNTs) in the matrix material was evaluated concurrently with the self-sensing abilities of the hybrid composite [18].

Self-sensing is achieved via the employment of the percolated electrical network within the matrix which performs as a sensor in the structure. The changes in the electrical properties of nano-composites and CFRPs, when subjected to load provide a direct measure for both strain and damage accumulation.

On the other hand, dielectric based methodologies have become one of the most interesting techniques for the on-line monitoring of changes that occur to physical and chemical properties of polymeric resins and their composites during the curing process. Through dielectric analysis the instantaneous degree of cure, cure rate, and viscosity evolution have been predicted [19-21]. Recently, the CNT dispersion process in epoxies has been related to the impedance of the system and has been successfully modeled as an equivalent RLC circuit [22, 23], however, little research effort has been devoted to the study of the impedance properties of nano-reinforcement composites and its relation to loading history and/or internal damage. Within the scope of this work is to enhance the resolving ability of the electrical based methodologies via the employment of AC configurations. These involve the study of the effect of damage in the hysteretic electrical behavior of carbon nanotube reinforced epoxy nano composites. In a parallel study, an Electrical Potential Mapping (EPM) technique was developed to pin-point artificial damage in CNT-enhanced matrix composite materials using DC resistance measurements, with a view to the development of an automated impedance mapping facility and its correlation to damage evolution in the structure.

2. Experimental

2.1. Materials

For the EPM (DC measurements), Carbon nanotube modified epoxy resin CFRPs were manufactured. 16-layer quasi-isotropic CFRPs with 0.5% w/w CNT modified epoxy matrix were manufactured. The first epoxy matrix used was the Araldite LY 5052/Aradur 5052 by Huntsman International LLC (Switzerland). Multi Wall Carbon Nanotubes (MWCNTs) by Arkema, France, were employed as additives in the epoxy matrix of the hybrid composites. MWCNTs were synthesized by Catalyzed Chemical Vapor Deposition (CCVD) and the tube diameter ranged from 10 to 15 nm, the tube length was more than 500 nm. CFRP laminated were produced using the infusion method. After curing, 60mmx60mm square specimens were cut from the laminates.

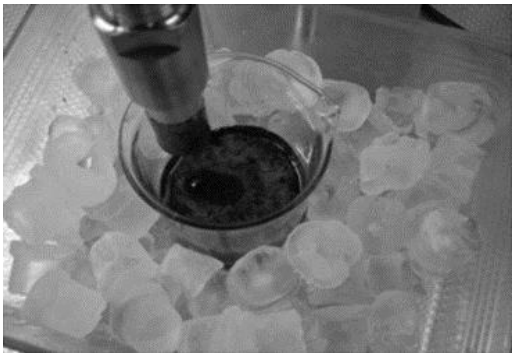

Figure 1. Sonication process.

For the hysteretic investigation (AC measurements), the Araldite LY 564 and Aradur 2954 by Huntsman Advanced Materials, Switzerland was employed for matrix. As for the reinforcement, MWCNTs were used. CNTs were identical to the EPM concept. In all cases, good dispersion quality of the CNTs in the epoxy matrix was achieved via sonication.

2.2. Processing of the nanocomposites: Sonication

In order to disperse the CNTs into the epoxy resin an ultrasonic mixer (UP400S, Hielscher) was used. CNTs and resin were carefully weighed and mixed together in a beaker. An ice bath was also used so as to avoid overheating of the polymer resin and introduction of defects on the CNTs surface,

Figure 1. CNTs were dispersed in the matrix using sonication for 4 hrs at 100% amplitude. At the end of this process the hardener was added to the modified resin and mixed using a mechanical agitator for about 10 minutes. At the end, the first mixture (Araldite LY 5052/Aradur 5052) transferred into silicon rubber molds and cured at 23 ^{o}C for one day and the second mixture (Araldite LY 564/ Aradur 2954) cured at 60 ^{o}C for 2 hours. Post curing of first and second systems was carried out at 100 ^{o}C for 4 hours and 120 ^{o}C for 4 hours respectively. It must be pointed out that the addition and the dispersion of the CNTs into the polymeric matrix resulted to an increase of the glass transition temperature (Tg) of the polymer. This phenomenon can be attributed to the interaction between the CNTs and the epoxy matrix [24].

2.3. Testing procedure

2.3.1. Impact damage/drilled open hole. For the EPM study, two damage concepts were investigated; impact damage and drilled hole. A 5 mm drilled hole, a 3 J and a 5 J blind impact damage were inspected. The circular notch was drilled using a diamond drill in the centre of the specimen. Dynamic impact tests were carried out using an Instron (CEAST 9340) drop-weight round impactor. Before the impact, the specimens were clamped on the testing machine. The performed impact energy levels did not lead to penetration of the employed composite laminates. In all cases, an Agilent multimeter was employed for the electrical resistance and electrical potential measurements. Regarding the resistance technique, the two-wire approach was adopted. For the electrical potential mapping, 100mA electrical current was injected by an external DC power supply.

2.3.2. Cycling Thermal Shock. Cyclic thermal shock was performed in order to simulate temperature changes which occur to aircraft structures. The specimens divided into four groups. The first group was undamaged and subsequently used as reference. Second, third and fourth group of samples subjected to a range of 30, 50 and 70 cycles, respectively. The temperature changes ranged from -30 ^{o}C to +30 ^{o}C. Samples remained at these temperatures for one hour.

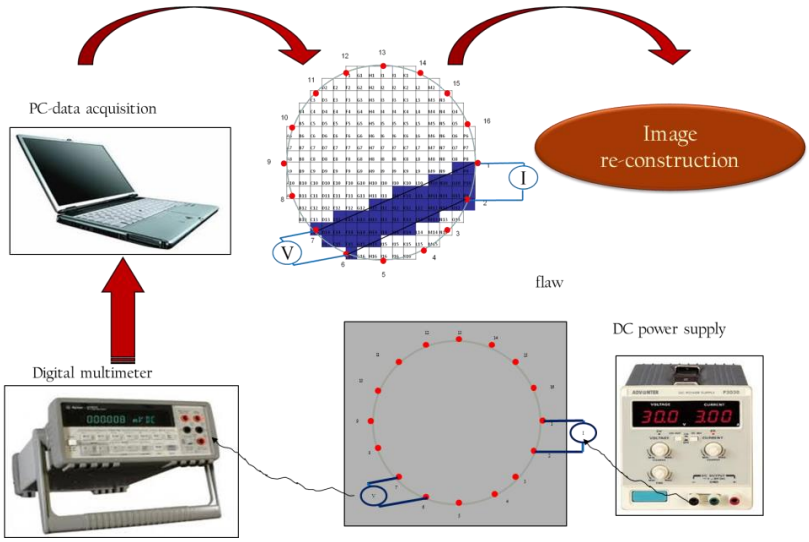

Figure 2. Experimental setup for EPM surface measurement.

2.3.3. Electrical Potential Mapping (EPM) system implementation. In Figure 2 the EPM experimental setup and the measurement protocol are depicted. 150 mA DC current was injected through an

electrical contact pair. The voltage between all the remaining electrical adjacent contact pairs was subsequently measured using the digital multimeter. The same measurement sequence was followed by moving the pair of the injecting electrodes and measuring the voltage at all the respective remaining electrical contacts.

As is shown in Figure 2, the electrical contacts on the surface of the investigated coupons draw a circle which was segmented in separated cells. In specific, a square of 16 × 16 cells was formed in excel. Every cell represents an average of electrical potential measurements. Further on, the two lines which connect the input and output pair of electrodes in the grid representation define the cells that will be include in the average of each cell. According to the employed protocol, when more than one third of the cell is included in between the lines, then this cell is included in the total average measurements.

2.3.4. Impedance (AC) measurements. An instrumentation of an AC power supply source (dual channel arbitrary/function generator AFG 3052C) and a two channel digital storage oscilloscope (TDS 2002C) supplied by Tektronix was developed, Figure 3. Silver conductive paint and silver conductive tape were used to achieve good electrical coupling between the sample surface and the electrodes.

In order to obtain the hysteresis curves, the power supply created a voltage waveform with constant amplitude of 21 Volts and a frequency that varied from 80 Hz to 2 kHz through the examined material. On the other hand oscilloscope's channel 1 and channel 2 recorded the inbound and outbound voltage waveform respectively. Then the two waveforms are plotted in the same graph in oscilloscope's screen. Finally phase-φ and amplitude from peak to peak were also displayed.

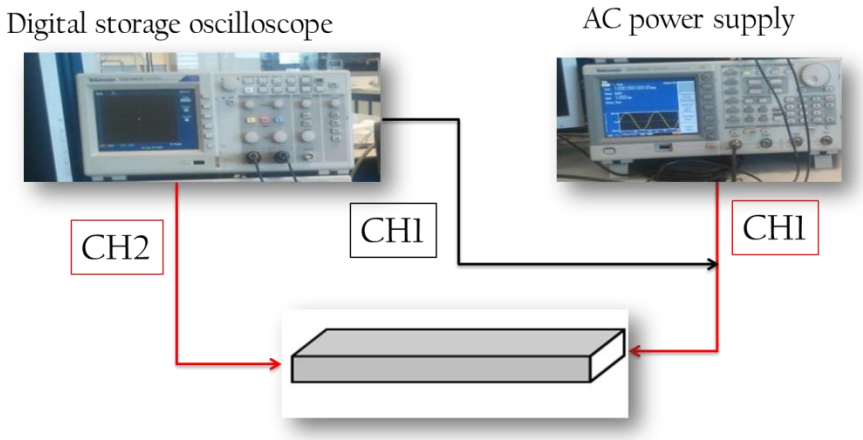

Figure 3. Experimental setup for the electrical (AC) measurements.

3. Results and Discussion

3.1. Electrical Potential Mapping (EPM)-DC measurements

Figure 4 depicts the damaged material with the 5 mm drilled hole. The differentiation in colour in the centre of the image represents the presence of the artificially induced drilled hole in the centre of the specimen.

Figure 5 displays the impacted plate against the employed NDE methods for the 3 J impact, which indicates that the damage is visible in the form of a semi-spherical dent at the impact site. As can be seen in Figure 5b, the induced damage by the round impactor is within the resolving power of the C-scan image. The exhibited color differentiation on the image indicates that measurements identify damage in the center of the specimen.

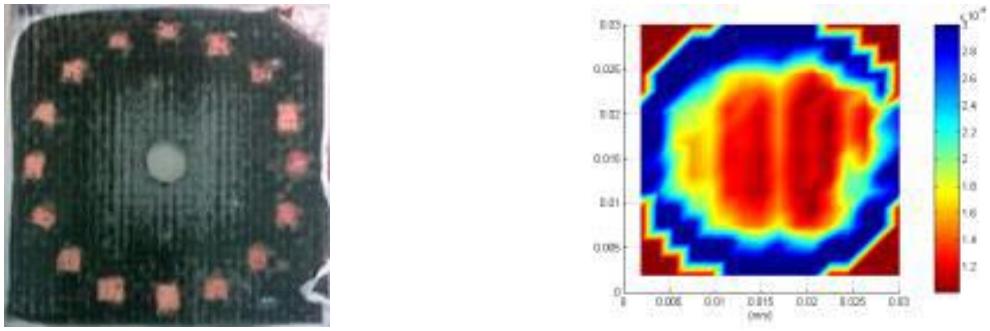

(a) (b)

Figure 4. (a) Cross-ply CFRP-5mm drilled hole (b) EPM image.

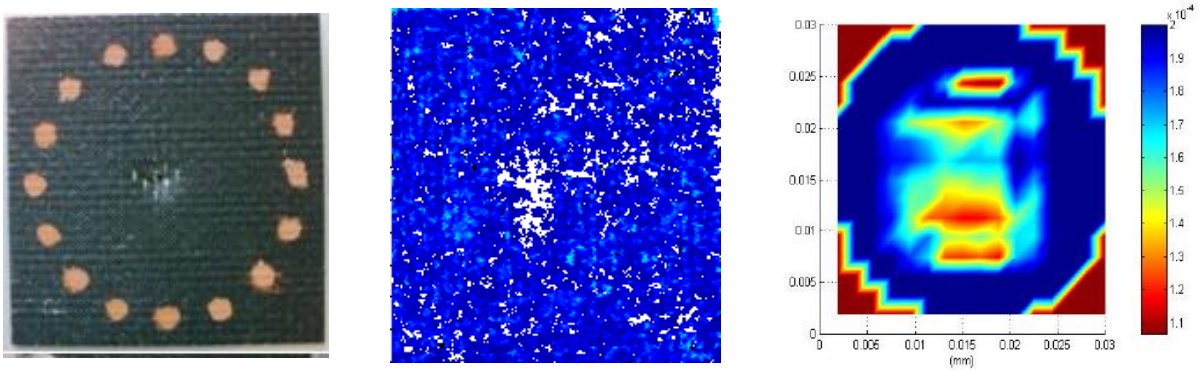

(a) (b) (c)

Figure 5. (a) Cross-ply a 3J impact damage (b) C-scan (c) EPM image.

In Figure 6a the 5 J LVI damaged specimen is presented. In this case, damage is barely or invisible to the naked eye. Figure 6b shows the caused impact damage through an amplitude C-scan image. Figure 6c shows the EPM image. Concerning the EPM image, the deterioration of the material is expected to be identified in the centre based on the ultrasonic testing.

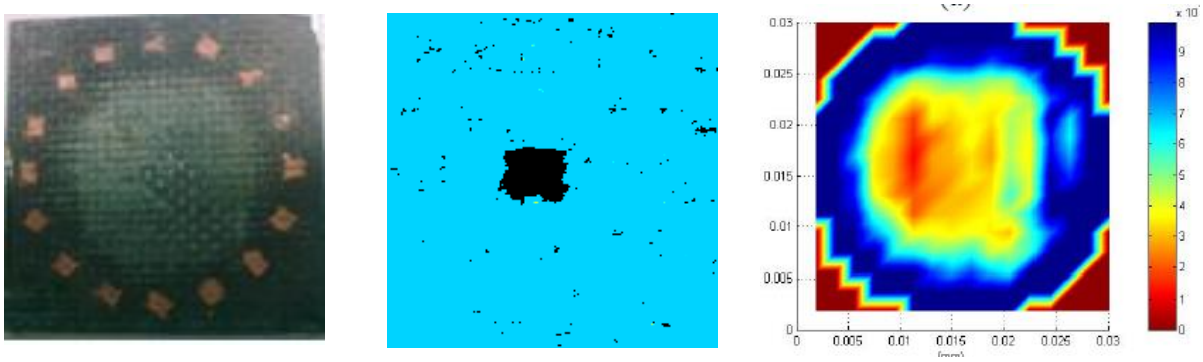

(a) (b) (c)

Figure 6. (a) Cross-ply a 5 J impact damage, (b) C-scan (c) EPM image.

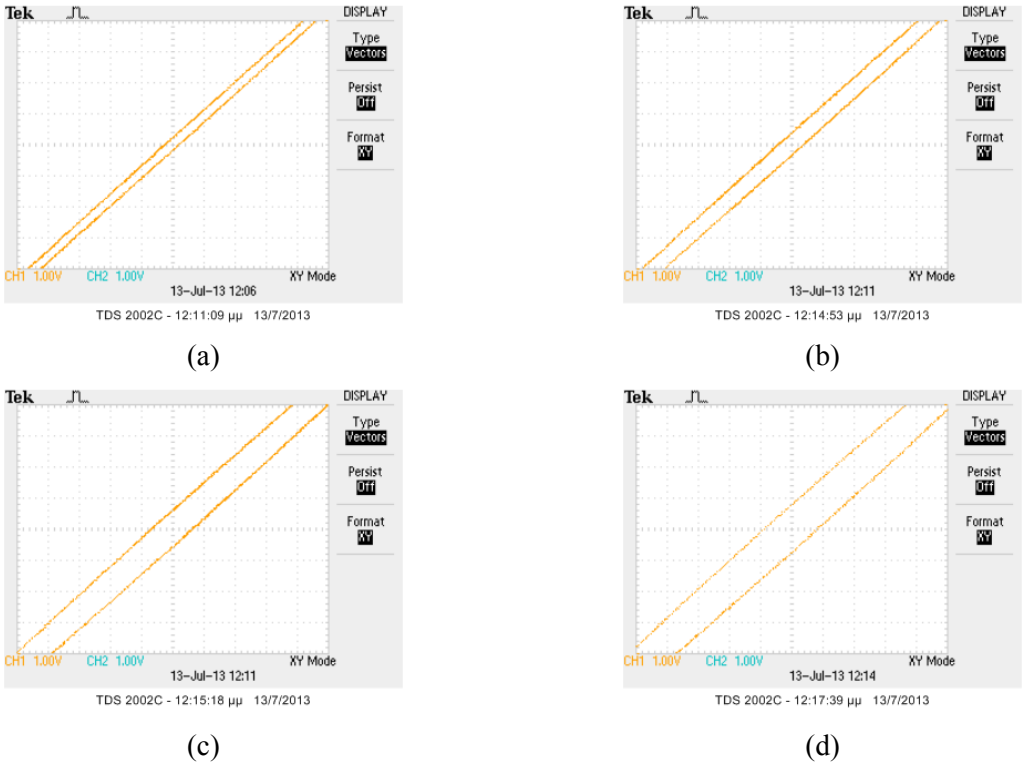

Figure 7. V-V curves for the specimen subjected to thermal shock (30 cycles) at: (a) 250Hz of AC voltage; (b) 450 Hz of AC voltage; (c) 750 Hz of AC voltage; (d) 1 kHz of AC voltage.

3.2. AC measurements

Four V-V curves were generated at 250, 450, 750 and 1000 Hz for every sample. Figure 7 presents the hysteretic electrical behavior of carbon nanotube reinforced epoxy nanocomposite that subjected to 30 cycles of thermal shock. As long as the material is under an electric field, CNTs act like dipoles. These dipoles are trying to orient to the direction of the electric field. As frequency of the AC increases dipoles cannot follow these changes properly, thus, wider hysteresis cycles can be observed. Moreover, changes in hysteresis cycles observed for the same frequency of AC voltage in different levels of damage. This becomes more obvious in the plots, Figure 8, where the V-V curves with 1 kHz for the four specimens are presented.

The measured phase delay (-) is increasing both with frequency and the level of damage for all observed systems. Phase delays are recorded for frequencies above approximately 200 Hz. This can be clearly distinguished in Figure 9 where phase-φ – frequency graphs are depicted for every sample with different levels of damage. Specimens subjected to 50 and 70 cycles of thermal shock show the largest difference in both in phase and drop rate of the phase delay when compared to the reference one.

4. Conclusions

The scope of the work described in this section was to examine the linear and non-linear electrical dependency of nano-composites to internal damage. Initially, an electrical potential mapping (EPM) system was developed with a view to identifying induced damage in composite laminates.

The implementation of the EPM technique proved its reliability and effectiveness in identifying both the notch and the impact induced damages in the laminates. The EPM algorithm identified

potential differences corresponding to the location of the drilled-hole and blind impact damage, moreover, the enhancement of the resolving ability of the electrical based methodologies via the employment of AC configurations was studied.

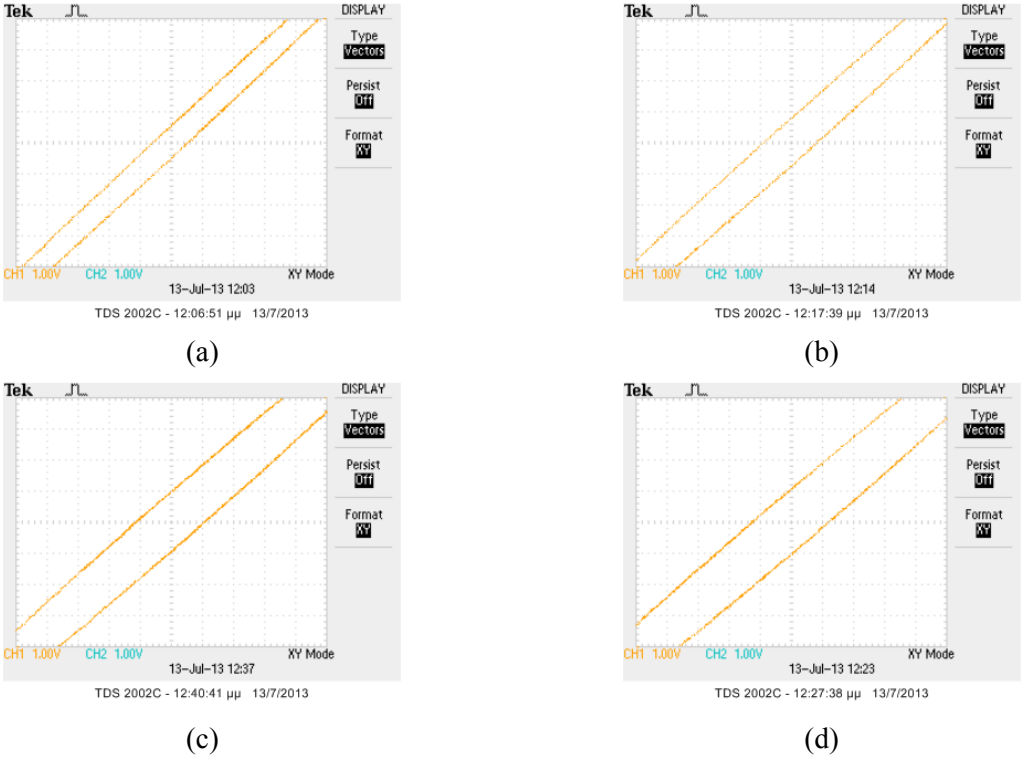

Figure 8. V-V curves generated using AC voltage with 1 kHz frequency for specimens subjected to thermal shock: (a) 0 cycles; (b) 30 cycles; (c) 50 cycles; (d) 70 cycles.

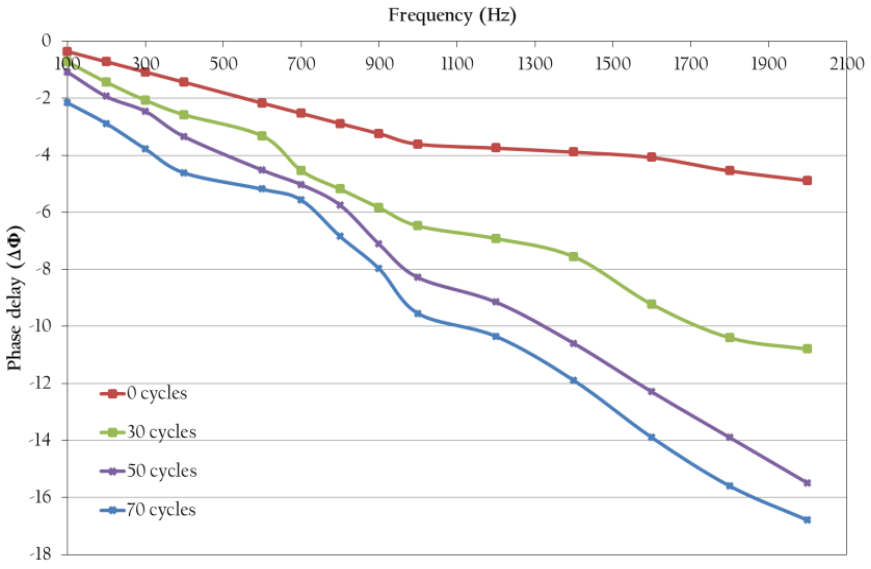

Figure 9. Phase-φ – frequency curves for four samples with different levels of damage.

The effect of damage in the hysteretic electrical behaviour of nano-enhanced reinforced composites was investigated. The results obtained from the AC voltage measurements indicate that the hysteresis curves become wider as the level of damage increases and a correlation between phase-φ and frequency of the AC voltage was achieved. Currently effort is being devoted in combining the aforementioned methodologies (AC and DC) for the accomplishment of a fully automated impedance mapping in order to increase the accuracy of the solution of the inverse problem by introducing a higher dimension to the problem (both measure and phase).

The implementation of the EPM technique proved its reliability and effectiveness in identifying both the notch and the impact induced damages in the laminates. The EPM algorithm identified potential differences corresponding to the location of the drilled-hole and blind impact damage, moreover, the enhancement of the resolving ability of the electrical based methodologies via the employment of AC configurations was studied.

The effect of damage in the hysteretic electrical behaviour of nano-enhanced reinforced composites was investigated. The results obtained from the AC voltage measurements indicate that the hysteresis curves become wider as the level of damage increases and a correlation between phase-φ and frequency of the AC voltage was achieved. Currently effort is being devoted in combining the aforementioned methodologies (AC and DC) for the accomplishment of a fully automated impedance mapping in order to increase the accuracy of the solution of the inverse problem by introducing a higher dimension to the problem (both measure and phase).

References

[1] Bauhofer W, Kovacs JZ, 2009, *Composites Science and Technology* **69** 1486–1498.
[2] Qian H, Greenhalgh ES, Shaffer MSP, Bismarck A, 2010, J. Mater. Chem 20 4751–4762.
[3] Rahmat M, Hubert P, 2011, *Composites Science and Technology* **72** 72–84.
[4] Ma PC, Siddiqui NA, Marom G, Kim JK 2010, *Composites: Part A* **41** 1345–1367.
[5] Spitalsky Z, Tasis D, Papagelis K, Galiotis C, 2010, *Progress in Polymer Science* **35** 357–401.
[6] Allaoui A, Bai S, Cheng HM, Bai JB, 2002, *Composites Science and Technology* **62** 1993–1998.
[7] Gojny FH, Wichmann MHG, Fiedler B, Kinloch IA, Bauhofer W, Windle AH, Schulte K, 2006, *Polymer* **47** 2036–2045.
[8] JSandler J, Shaffer MSP, Prasse T, Bauhofer W, Schulte K, Windle AH, 1999, *Polymer* **40** 5967–5971.
[9] Huang Y, Li N, Ma Y, Du F, Li F, He X, Lin X, Gao H, Chen Y, 2007, *Carbon* **45** 1614–1621.
[10] Zheng W, Wong SC, 2003, *Composites Science and Technology* **63** 225–235.
[11] Sandler JKW, Kirk JE, Kinloch IA, Shaffer MSP, Windle AH, 2003, *Polymer* **44** 5893–5899.
[12] Shindo Y, Kuronuma Y, Takeda T, Narita F, Fu SY, 2012, *Composites Part B* **43** 39-43.
[13] Fiedler B, Gojny FH, Wichmann MHG, Bauhofer W, Schulte K, 2004, *Sci Mat* **29** 81–94.
[14] Nofar M, Hoa SV, Pugh MD, 2009, *Compos Sci Technol* **69** 1599–1606.
[15] Thostenson ET, Chou TW, 2006, *Adv Mater* **18** 2837–2841.
[16] Park M, Kim H, Youngblood JP, 2008, *Nanotechnology* **19** 055705 (7pp).
[17] Kang I, Schulz MJ, Kim JH, Shanov V, Shi D, 2006, *Smart Mater. Struct.* **15** 737–748.
[18] Grammatikos SA, Paipetis AS, 2012, *Composites: Part B* **43** 2687–2696.
[19] Kim D, Centea T, Nutt SR, 2014, *Composites Science and Technology* **102** 132–138.
[20] Maistros GM, Partridge IK, 1998, *Composites: Part B* **29B** 245–250.
[21] McIlhagger A, Brown D, Hill B, 2000, *Composites: Part A* **31** 1373–1381.
[22] Gkikas G, Saganas C, Grammatikos SA, Maistros GM, Barkoula NM, Paipetis AS, 2012, *Sensors and Smart Structures Technologies for Civil, Mechanical, and Aerospace Systems*.
[23] Gkikas G, Saganas C, Grammatikos SA, Aggelis DG, Paipetis AS, 2012, *Smart Sensor Phenomena, Technology, Networks, and Systems Integration* (7pp).
[24] Gkikas G., Barkoula N.-M., Paipetis A. S. 2012 *Composites: Part B* **43** 2697–2705.